CIRP Annals - Manufacturing Technology 70 (2021) 37–40

Contents lists available at ScienceDirect

CIRP Annals - Manufacturing Technology

journal homepage: https://www.editorialmanager.com/CIRP/default.aspx

Machinability exploration for high-entropy alloy FeCrCoMnNi by ultrasonic vibration-assisted diamond turning

Lin Zhang, Takeshi Hashimoto, Jiwang Yan (2)*

Department of Mechanical Engineering, Keio University, Yokohama 223-8522, Japan

ARTICLE INFO

Article history:
Available online 19 May 2021

Keywords:
Ultrasonic
Machinability
High-entropy alloy

ABSTRACT

High-entropy alloy (HEA) is an emerging alloy which consists of five or more metallic elements with equimolar concentrations and exhibits excellent mechanical properties at cryogenic temperature. However, its machinability is almost unknown. In this study, high frequency one-dimensional ultrasonic vibration-assisted diamond turning (UVDT) experiments were conducted on an FeCrCoMnNi-based HEA to investigate the micro-nanoscale material removal mechanisms. Compared with conventional diamond turning, UVDT produced thinner chips, lower cutting forces, less tool wear and better surface integrity. Due to the ultrasonic vibration-assisted burnishing effect, surface scratches were significantly eliminated. A freeform surface was test-fabricated with optical-level finish.

1. Introduction

Conventional metal alloys are based on one or two main elements in which a small amount of other elements is added to tailor the microstructure and mechanical/chemical performance. In contrast, high-entropy alloy (HEA) is a new member of metal alloy family, which contains five or more principal elements with equimolar ratios [1]. Owing to its unique atomic and crystallographic structure, HEA exhibits various superiorities over conventional intermetallic compounds. For instance, single-phase HEA FeCrCoMnNi exhibits outstanding strength-ductility trade-off, especially at cryogenic temperature [2], thus has potential applications in space technology and so on. However, as all the elements are ferrous transition metals having strong chemical affinity with diamond, diamond turning of FeCrCoMnNi has been considered impossible. Though recent studies have focused on HEA machining [3], its machinability is still unclear.

Elliptical ultrasonic vibration has been demonstrated to be effective to suppress chemical wear of diamond tools in cutting steel materials, but the cutting performance depends strongly on the cutting speed [4,5]. In this study, one-dimensional ultrasonic vibration-assisted diamond turning (UVDT) of HEA was explored. Chip morphology, surface topography, cutting forces, subsurface microstructural changes and tool wear were investigated. The effect of ultrasonic tool vibration on the cutting mechanism was clarified. A freeform optical microstructure was fabricated to demonstrate the feasibility of durable diamond turning of HEAs.

2. Material and methods

A face-centred-cubic (FCC) HEA, FeCrCoMnNi, was used as workpiece material. As schematically shown in Fig. 1(a), the material

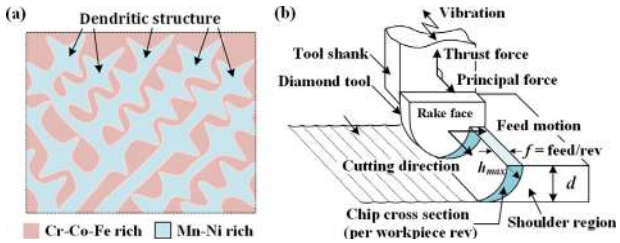

Fig. 1. Schematic diagrams of (a) HEA microstructure and (b) UVDT.

microstructure is featured by Mn-Ni dendrites in a Cr-Co-Fe matrix. A cylindrical ingot was produced by arc melting, agitating, solidifying and remelting in pure Ar atmosphere before drop casting. The purity of each constituent material was >99.9%. The ingot was sliced into rectangular samples ($20 \times 25 \times 4\,mm^3$) by wire electric discharge machining. The heat-effected layer on the workpiece surface was removed by lapping and polishing with a diamond slurry before cutting experiments.

An ultraprecision lathe Nanoform X (AMETEK Precitech Inc., USA) with XZBC four-axis simultaneous control was used. The lathe has an air spindle and hydrostatic rotary/linear tables enabling a nanometric step resolution. A single-crystal diamond tool (nose radius 1.0 mm, rake angle 0°, relief angle 8°, edge radius ~50 nm) was utilized. An ultrasonic tooling system UTS2 (Son-X Company, Germany) was mounted to the lathe to vibrate the tool in the cutting direction with a resonance amplitude of 1.0 μm at a frequency of 101.68 kHz. In the case of one-dimensional vibration, the resulting surface roughness is independent of cutting speed, thus uniform surface quality can be obtained even in face turning. In addition, the vibration frequency used in this study is several times higher than that used in previous studies (20–40 kHz) [4,5], thus better cutting performance is expectable. A piezoelectric dynamometer, Kistler 9256C2, was used to

* Corresponding author.
E-mail address: yan@mech.keio.ac.jp (J. Yan).

https://doi.org/10.1016/j.cirp.2021.04.090
0007-8506/

collect the cutting forces. In order to collect cutting chips for observation, the experiments were conducted under dry conditions.

Fig. 1(b) shows a schematic model of UVDT. In the experiment, spindle rotation rate was set to 100 rpm and depth of cut d to 5 μm. Tool feed rate f was changed from 1 to 10 μm/rev, accordingly the maximum undeformed chip thickness h_{max} varied from about 0.1 to 1 μm. For comparison, conventional diamond turning (CDT) was also conducted under the same conditions. After cutting, scanning electron microscopy (SEM), energy-dispersive X-ray spectroscopy (EDS), X-ray diffraction (XRD), electron backscatter diffraction (EBSD) and cross-sectional transmission electron microscopy (TEM) were used to characterize the chip morphology and surface/subsurface properties. The cross-sectional samples for TEM observation were prepared by focused ion beam (FIB) machining and thinned to a thickness of ~100 nm.

3. Results and discussion

3.1. Surface topography and defect analysis

Fig. 2 illustrates SEM images of the surfaces machined with and without tool vibration. Some surface defects were extracted and enlarged as insets in Fig. 2(a) and (c). For CDT, lots of micro pits, particle adhesions and scratches were found (Fig. 2(a)-(b)). In contrast, surface defects of UVDT were distinctly fewer. Although scratches and vibration tool marks perpendicular to the cutting direction existed when $f > 4$ μm/rev (Fig. 2(c)), when $f < 4$ μm/rev, however, surface defects completely disappeared, and a smooth surface was obtained (Fig. 2(d)). The surface roughness of CDT and UVDT at different feed rates is shown in Fig. 3. Compared with CDT, the surface roughness of UVDT was reduced by a factor of 10–18.

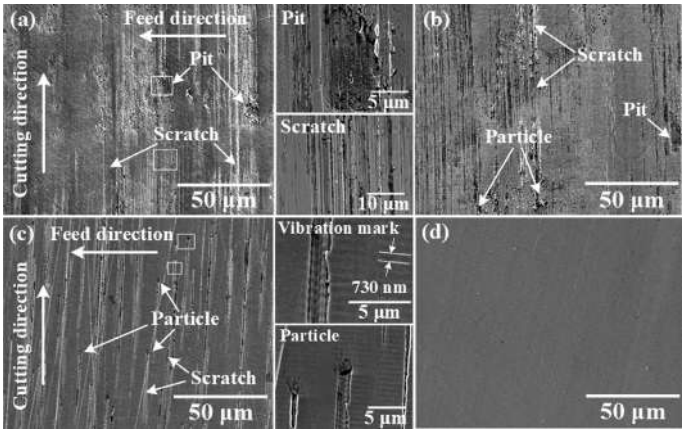

Fig. 2. SEM images of surfaces machined by CDT at (a) $f = 10$ μm/rev, (b) $f = 1$ μm/rev, and UVDT at (c) $f = 10$ μm/rev, and (d) $f = 1$ μm/rev.

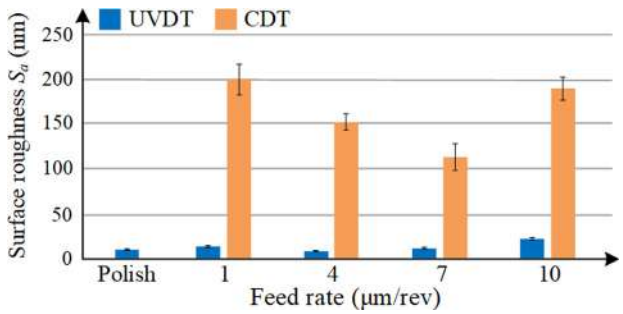

Fig. 3. Surface roughness of CDT and UVDT at different feed rates.

Fig. 4 shows EDS analysis results of typical defects on the machined surfaces in Fig. 2(b) and (c). In Fig. 4(a), deep scratches were generated by the movement of particles in the workpiece material. EDS results indicated that the particles were rich in Cr, which has higher hardness than other elements (Mohs hardness: Cr 8.5, Co 5.0, Mn 6.0, Fe 4.0, Ni 4.0). In Fig. 4(b), it is seen that scratches only occur for some specific zones. The binary image and element mapping indicated that the scratches were originated at the dendrite-matrix boundaries and extended across the dendritic regions with the movement of diamond tool. Then the hard particles were embedded at the end of the scratches on the machined surface.

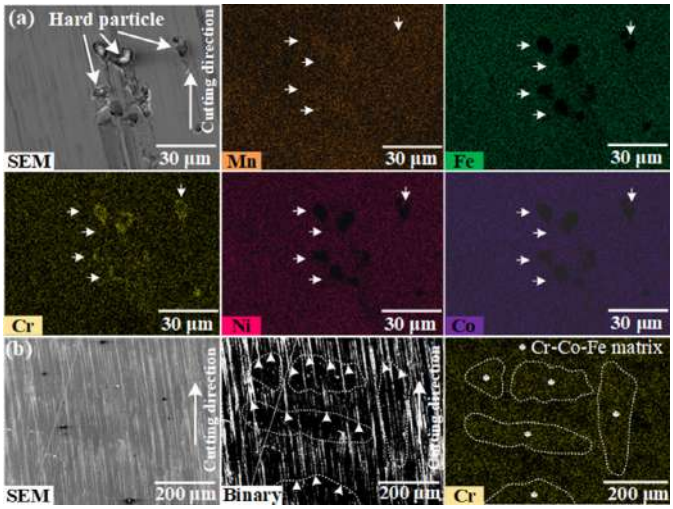

Fig. 4. EDS analysis for surface defects: (a) CDT at $f = 1$ μm/rev, and (b) UVDT at $f = 10$ μm/rev.

3.2. Chip morphology

Fig. 5 shows SEM images of cutting chips with and without tool vibration at a feed rate of 1 μm/rev. In Fig. 5(a), the chips are short and thick (thickness ~3.2 μm), having lamella structures on one side, like those in cutting other metals [6], and micro pits and scratches on the other side. In Fig. 5(b), the chips are thin (thickness ~140 nm) and continuous with wrinkling on chip edge, which might be due to squeezing-induced local elongation of the chip. There were periodic vibration marks on one side of the chip, which were generated by tool vibration, and lamella structures on the other side. The shear angle estimated from the chip thickness increased from 1.7° in CDT to 35.4° in UVDT. The remarkable increase of shear angle indicated that UVDT reduced the chip thickness, restrained the friction between the rake face and chip [6], and in turn, improved the machinability of the material.

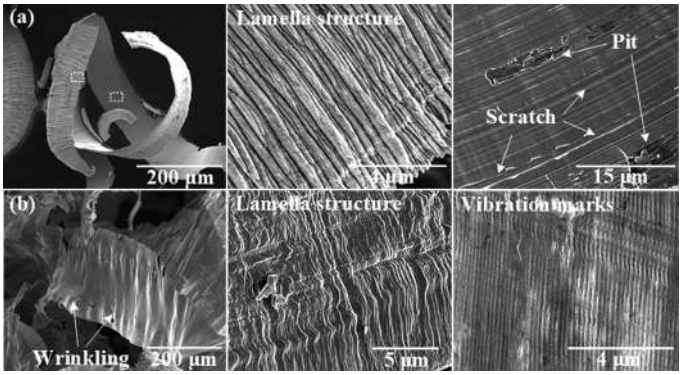

Fig. 5. SEM images of cutting chips from (a) CDT and (b) VUDT at $f = 1$ μm/rev.

3.3. Cutting force

Fig. 6 shows the change of the mean values of cutting forces in CDT and UVDT. For CDT, thrust force F_t was always larger than principal force F_c. It was noted that F_t increased when the cutting test number (n) increased from 1 to 4 (feed rate from 10 to 1 μm/rev). This increase in cutting forces might be due to the significant increase of tool wear with cutting distance in CDT, which will be experimentally

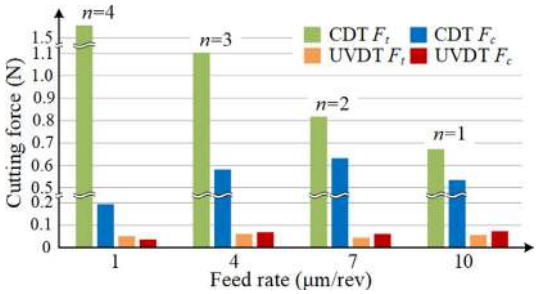

Fig. 6. Cutting forces for CDT and UVDT at different feed rates.

confirmed in Section 3.7. For UVDT, however, both F_c and F_t were reduced by a factor of more than 10, although the peak force might be considerably larger than the mean force in UVDT because the measurement result of the mean force depends on the sampling rate (4.8 kHz in this study). The reduction of cutting force agrees well with the increase of shear angle and decrease of chip thickness shown in Section 3.2. In addition, it is noteworthy that for UVDT, F_c was larger than F_t (except for the condition $f = 1$ μm/rev), and the cutting force did not change obviously with cutting test number n. This is a strong indication of that tool wear was insignificant in UVDT.

3.4. Surface micro hardness

To explore the mechanical property of the finished surface, nanoindentation tests were conducted using a Berkovich indenter at a maximum load of 10 mN. The indentation depth was 250 ~ 290 nm, which was close to the thickness of the subsurface layer affected by cutting. In order to eliminate random error, twenty indentations were made for each surface and the results were averaged. As shown in Fig. 7, compared with the initial surface, the machined surfaces show a hardness increase (~50%) for both CDT and UVDT. The UVDT surface is slightly harder than the CDT surface. For CDT, the surface hardness increase was mainly caused by the work hardening effect of workpiece material under a high negative rake angle of a worn tool. In UVDT, the tool wear was insignificant, thus the main cause of the surface hardness increase should be the ultrasonic impacts of the tool tip.

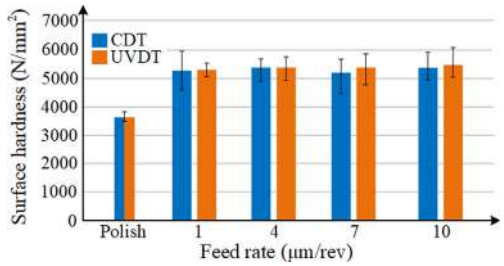

Fig. 7. Comparison of hardness of CDT and UVDT machined surfaces.

3.5. Change in crystal structure and grain size

To investigate possible change in crystalline structure induced by diamond turning, XRD analysis was conducted on the as-cast and diamond-turned surfaces and the patterns were shown in Fig. 8. The results only showed typical peaks for the FCC crystalline structure,

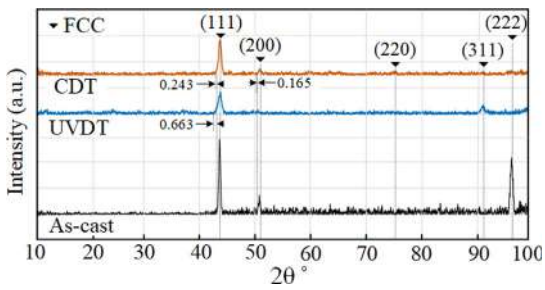

Fig. 8. XRD patterns for the as-cast, CDT and UVDT surfaces.

indicating that neither CDT nor UVDT had changed the crystal structure of the as-cast HEA. However, after diamond turning, the intensity of (111) peak decreased while that of (220) and (311) increased. It might be due to the grain refinement and reorientation caused by diamond turning, which resulted in weakened peak intensity. The increase of half-peak width of the peaks after diamond turning also indicated the possibility of grain refinement [7].

Fig. 9 shows EBSD images illustrating the microstructure evolution of the machined surfaces by UVDT. The grain size was reduced from tens of micrometres to hundreds of nanometres over a large area. The grain refinement increased the fraction of grain boundaries as well as the resistance to plastic deformation, leading to higher strength and hardness [8]. For CDT, due to the surface was very rough, clear EBSD images could not be obtained.

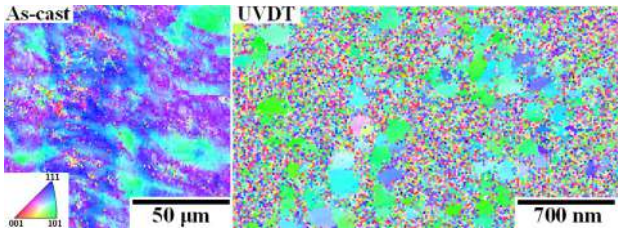

Fig. 9. EBSD images of the as-cast and UVDT machined surface.

3.6. Subsurface microstructure

Fig. 10(a) shows TEM image of the subsurface layer of the as-cast HEA. Large grains are clearly found under the surface with minor defects on the grain boundaries. The inset is the selected area electron diffraction (SAED) pattern, indicating a well-defined FCC crystalline structure. Fig. 10(b) shows TEM image of the subsurface layer of UVDT surface at 4 μm/rev. A layer of refined grains is identified under the machined surface. Meanwhile, mechanical twins (MTs), stacking faults (SFs), and dislocation tangles (DTs) were found along different directions in the near surface layer. It might be due to the low stacking faults energy of HEA and dislocation plugging during plastic deformation. These results demonstrate that grain refinement and reorientation might have occurred, and the new grain boundaries and crystal defects improved the resistance of the surface layer to further plastic deformation, and enhanced the hardness of the finished surface in UVDT.

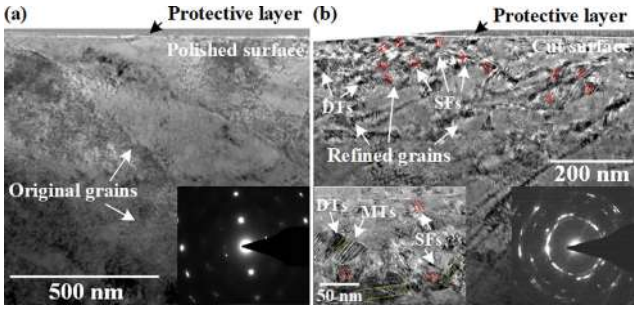

Fig. 10. TEM images of the subsurface layers of (a) as-cast, and (b) UVDT at $f = 4$ μm/rev.

3.7. Tool wear

The tool edges were observed after CDT and UVDT for a cutting distance of 88 m. Fig. 11 shows SEM images of the tools taken from the rake face and flank face sides, respectively. As seen in Fig. 11(a), severe flank wear was found for CDT, causing a ~4.3 μm recession of the cutting edge. In addition, rake wear and material adhesion occurred. For the UVDT, the tool wear was distinctly small (width of flank wear < 1 μm), as shown in Fig. 11(b). The tool wear suppression in UVDT can be attributed to the vibration-induced reduction of effective contact time between the tool and the workpiece [9]. By considering vibration frequency, amplitude and cutting speed, the

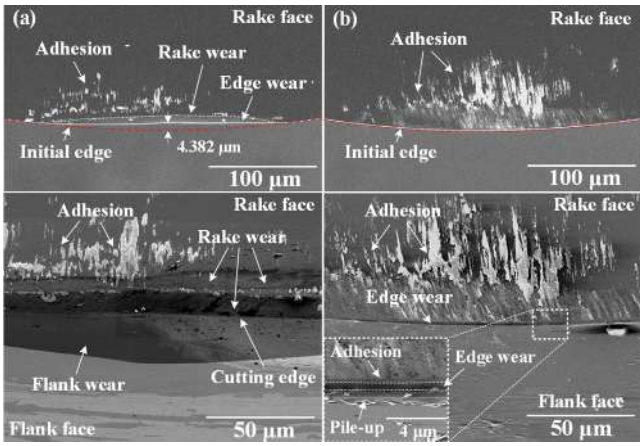

Fig. 11. SEM images of tool edges after cutting: (a) CDT and (b) UVDT.

tool-workpiece contact ratio (TWCR) was estimated [10]. In UVDT, the TWCR was reduced to about 13% ~ 20% of CDT. In addition, from the inset, a uniform thin layer of material adhesion covering the rake surface was identified, which might be a result of interfacial ultrasonic impacts. This thin adhesion layer might have also protected the tool rake face from erosion by a fresh chip surface.

4. Scratch elimination mechanism

As shown in Section 3.1, surface scratch is a major problem for HEA machining. The mechanism for scratch formation in CDT is schematically shown in Fig. 12(a). A Cr-rich hard particle near the tool tip is driven forward by the tool tip and scratches along the cutting direction, leading to a deep groove on the surface. The particle is finally embedded into the machined surface at the end of the groove. When undeformed chip thickness is small, the tool edge radius becomes relatively large, inducing a highly negative effective rake angle. The burnishing effect generated by the negative effective rake angle may embed some hard particles and reduce scratches. However, some hard particles will keep staying with the edge, thus scratches cannot be completely eliminated in CDT. In contrast, as seen from the SEM image of the machined surface in Fig. 2(d), scratch formation was completely eliminated for UVDT. As shown in Fig. 12(b), hard particles cannot stay with the tool edge under ultrasonic vibration, and will be smoothly embedded inside the finished surface by the high-frequency impacts from the tool. As a result, ultrasonic vibration-assisted nanoscale burnishing effect generates a smooth surface on HEA.

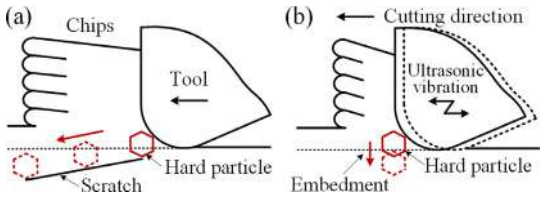

Fig. 12. Schematic models for (a) scratch formation in CDT and (b) scratch elimination in UVDT.

5. Microstructured surface fabrication

To demonstrate the feasibility of durable machining by UVDT for surface structuring on HEA, a sinusoidal free-form surface was generated, the shape of which is expressed as:

$$z_w(x_w, y_w) = A_x \sin(2\pi f_x x_w) + A_y \sin(2\pi f_y y_w) \quad (1)$$

where A_x and A_y are amplitude, and f_x and f_y are spatial frequency in x and y direction, respectively. In the demonstration, the amplitude and spatial frequency are set as $A_x = A_y = 1.2\ \mu m$ and $f_x = f_y = 1.0\ mm^{-1}$. An optical image and a 3D topography of the machined surface are presented in Fig. 13(a) and (b). A 3D local surface topography after removing the sinusoidal component is given in Fig. 13(c). Although there are periodical tool feed marks and some slight fluctuations along the cutting direction, which may be due to the tool vibration, a smooth surface of 5.162 nm S_a was obtained with optical-level finish. Fig. 13(d) shows 2D cross-sectional profiles measured along the A-A and B-B directions indicated in Fig. 13(b). The 2D profiles show that the form error is smaller than ~ 50 nm. No detectable tool wear was found by SEM observation after the machining of this sample.

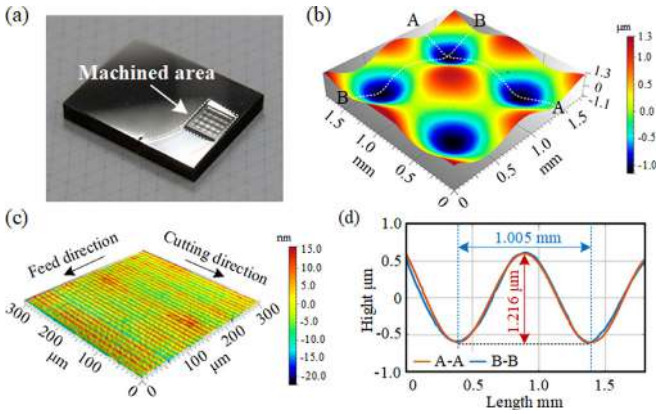

Fig. 13. Sinusoidal surface machined by UVDT: (a) optical image, (b) 3D topography, (c) 3D local topography, and (d) 2D profiles.

6. Conclusions

The mechanism of high frequency one-dimensional ultrasonic vibration-assisted diamond turning (UVDT) of high-entropy alloy FeCrCoMnNi was explored. Results showed that UVDT reduced chip thickness, cutting forces, and tool wear and improved surface integrity. TEM and EBSD observations confirmed the occurrence of grain refinement in the near surface layer. The tool wear was significantly suppressed due to the vibration-induced reduction of tool-workpiece contact time. The impact-induced thin layer of material adhesion on the tool edge might have also protected the tool from erosion wear by fresh chip surfaces. The ultrasonic vibration-assisted nanoscale burnishing effect could completely eliminate scratch formation on the machined surface. The feasibility of free-form surface generation on HEA by the UVDT method was demonstrated.

Declaration of Competing Interest

The authors declare that they have no known competing financial interests or personal relationships that could have appeared to influence the work reported in this paper.

References

[1] Yeh JW, Chen SK, Lin SJ, Gan JY, Chin TS, Shun TT, Tsau CH, Chang SY (2004) Nanostructured High-Entropy Alloys with Multiple Principal Elements: Novel Alloy Design Concepts and Outcomes. *Advanced Engineering Materials* 6(5):299–303.
[2] Gludovatz B, Hohenwarter A, Catoor D, Chang EH, George EP, Ritchie RO (2014) A Fracture-Resistant High-Entropy Alloy for Cryogenic Applications. *Science* 345 (6201):1153–1158.
[3] Huang Z, Dai Y, Li Z, Zhang G, Chang C, Ma J (2020) Investigation on Surface Morphology and Crystalline Phase Deformation of $Al_{80}Li_5Mg_5Zn_5Cu_5$ High-Entropy Alloy by Ultra-Precision Cutting. *Materials & Design* 186:108367.
[4] Moriwaki T, Shamoto E (1991) Ultraprecision Diamond Turning of Stainless Steel by Applying Ultrasonic Vibration. *CIRP Annals - Manufacturing Technology* 40 (1):559–562.
[5] Shamoto E, Moriwaki T (1999) Ultaprecision Diamond Cutting of Hardened Steel by Applying Elliptical Vibration Cutting. *CIRP Annals - Manufacturing Technology* 48(1):441–444.
[6] Shamoto E, Moriwaki T (1994) Study on Elliptical Vibration Cutting. *CIRP Annals - Manufacturing Technology* 43(1):35–38.
[7] Zhang W, Ma Z, Zhao H, Ren L (2021) Breakthrough the Strength-Ductility Trade-Off in a High-Entropy Alloy at Room Temperature Via Cold Rolling and Annealing. *Materials Science and Engineering: A* 800:140264.
[8] Yan J, Okuuchi T (2019) Chip Morphology and Surface Integrity in Ultraprecision Cutting of Yttria-Stabilized Tetragonal Zirconia Polycrystal. *CIRP Annals - Manufacturing Technology* 68(1):53–56.
[9] Song Y, Nezu K, Park C, Moriwaki T (2009) Tool Wear Control in Single-Crystal Diamond Cutting of Steel by Using the Ultra-Intermittent Cutting Method. *International Journal of Machine Tools and Manufacture* 49(3):339–343.
[10] Nath C, Rahman M (2008) Effect of Machining Parameters in Ultrasonic Vibration Cutting. *International Journal of Machine Tools & Manufacture* 48(9):965–974.